SPECIFIC ATM-MEDIATED PHOSPHORYLATION DEPENDENT ON RADIATION QUALITY

Mary K. Whalen, Sukhleen K. Gurai, Hengameh Zahed-Kargaran and Janice M. Pluth*

Lawrence Berkeley National Laboratory, Life Sciences Division, One Cyclotron Road, Building 74, Berkeley, CA 94720, USA

---

*Corresponding author:
Phone: 510-486-5799
Fax: 510-486-6816
E-mail: jmpluth@lbl.gov

X Pages of text
1 Table
9 Figures
2 Pages of figure legends

KEYWORDS: DNA damage repair, phospho-protein kinetics, γH2AX foci, pATF2, pSMC1, Low LET, high LET

RUNNING TITLE: Radiation Quality Predicts ATM Dependent Phosphorylation Level

Whalen, M.K. Gurai, S.K. Zahed-Kargaran H. Pluth, J.M. Variable ATM-Mediated Phosphorylation Dependent on Radiation Quality. Radiat. Res.

Abstract

To determine whether the physical differences between high- and low-LET radiation are reflected in the biological responses of exposed cells, we detailed phospho-protein profiles of three proteins functional in radiation repair and signal transduction. Detailing γH2AX, pATF2 $Ser^{490/498}$ and pSMC1 Ser^{957} kinetics following X-ray and iron-ion exposure also provides a window into understanding the underlying cellular responses. Phosphorylated forms of these proteins have been documented to co-localize at sites of double strand breaks (DSBs) after low-LET exposures, and two of these phosphorylations, pATF2 and pSMC1, are specifically ATM dependent. Flow cytometry-based methods were used to quantify total levels of each phospho-protein at various times after radiation. As expected, we observed a greater induction and persistence in γH2AX after iron-ion (high-LET) exposure as compared to X-ray (low-LET). In contrast, pATF2 and pSMC1 showed markedly lower induction levels following Fe exposure as compared to equivalent doses of X-ray. Quantification of pATF2 and pSMC1 foci revealed fewer cells containing foci, and fewer foci per cell after iron-ion compared to X-ray exposure. These findings suggest that ATM responds to DSBs induced by high-LET radiation differently from DSBs induced by low-LET radiation.

INTRODUCTION

Double-strand breaks (DSBs) are the primary toxic lesion induced by ionizing radiation, although many other types of damages such as single strand breaks (SSBs), base-pair damage and oxidation of proteins and DNA also occur (*1, 2*). Unrepaired or misrepaired lesions can lead to mutations and genomic instability. Damage and repair processes induced within a cell cause a complex cascade of signaling events that in many cases involve phosphorylation of various proteins. Protein phosphorylation is a key regulatory event that can activate or deactivate protein function by changing interactions and/or sub-cellular localization and thus the inherent activity in critical biochemical pathways. Initiation of this signaling cascade following damage can influence a number of different cellular processes, including cell cycle checkpoints, transcription, repair, senescence and apoptosis. Three proteins are primarily involved in the initiation of phosphorylation events after damage, ataxia telangiectasia mutated protein (ATM), ataxia telangiectasia and RAD3-related protein (ATR), and DNA-dependent protein kinase catalytic subunit (DNA-PKcs) (*3-5*). These proteins have both unique and overlapping roles in response to ionizing radiation and phosphorlyate H2AX in response to damage (*6*). ATM has been shown to have a unique role in cell cycle regulation and activation of homologous recombination repair (HRR) (*6, 7*), ATR to be important in replication stress response (*8*), and DNA-Pkcs to play a key role in activation of proteins involved in non-homologous end joining (NHEJ) (*9, 10*).

DSBs differ in their complexity, with more complex types of damage occurring after high-linear energy transfer (LET) exposures than after low-LET radiation exposures (*11-13*). High-LET radiation deposits a large amount of energy in a small distance,

causing dense ionizations along a track. Low-LET radiations, however, deposit their energy more sparsely within a cell (*11*). Damage from high-LET radiation has been shown to induce multiple damaged sites or complex breaks, defined as two or more damages in a single turn of the DNA helix (*14*). The ratio of complex to simple breaks has been shown to increase with LET, and the complexity of the DSB has also been shown to correlate with DSB rejoining kinetics (*15, 16*). In addition to the direct track of ionizations from a high-LET particle, there are also δ rays emanating from this main track, which result in exposures similar to that of a low-LET radiation. Thus δ rays provide an additional dose to the cell, which is important to consider when understanding the biological effects of these types of radiations (*17-19*). Generally high-LET exposures have been shown to have an average relative biological effectiveness (RBE) of ~20, (depending on the biological endpoint being studied, they range from 2 to 40), which peaks at a LET of ~100 keV/μm (*20, 21*). However, an RBE of only 1.8 has been determined for the number of DSBs induced by iron-ions as compared to X-ray (*14, 22*). Thus an unanswered question to date is how the RBEs for some biological endpoints can be so large when the RBE for DSBs is so small. The differences in the proportions of different types of damages and the distribution of the energy deposited after low- and high-LET radiation exposures may result in distinct biological responses that are dependent on the radiation quality. Detailing the signal transduction events at various times after high-LET radiation exposure may aid in understanding this disparity in RBEs. Astronauts are exposed to high-LET radiation in their travels in space, and proposed future missions will entail longer exposures, thus a better understanding of the cellular effects of high-LET is especially relevant in determining the risks for these individuals.

H2AX is a variant of H2A and represents from ~2 to 25% of the total H2A depending on cell lineage (*23*). After DSB damage, H2AX is rapidly phosphorylated on residue 139 near its carboxy terminus, and the phosphorylated form has been designated γ–H2AX (*24*). γ–H2AX forms very rapidly in regions surrounding the DSB and can encompass up to 2 Mbp surrounding the break (*24*). This phosphorylated protein has been studied extensively because of the strong correlation between the number of microscopically detected γ–H2AX foci and the number of DSBs that form after irradiation (*25, 26*). Some caution must be taken in directly correlating the number of γ–H2AX foci with the number of radiation-induced DSBs, since γ–H2AX can also occur during normal cellular processes. For example, γ–H2AX occurs during V(D)J recombination, apoptosis, senescence and to a greater degree in S and G2 phases than would be expected based on DNA content (*27, 28*). In addition, more recent studies have shown that misrejoined DNA retains γ–H2AX at the sites incorrectly rejoined DNA (*29*). Detailed CHIP-based studies have also revealed that γ–H2AX is not directly at the sites of DSBs (within 1-2 kb) but rather flanks the DSB (*24*). However, even given these caveats, in general the numbers of γ–H2AX foci at early times after repair in G1 cells, has proven to be a very sensitive indicator of the number of DSBs induced after irradiation.

Activating Transcription Factor 2 (ATF2) was originally identified as a transcription factor regulated by JNK/p38 that is involved in the cellular response to stress (*30, 31*). More recently it has been shown to have a role in DSB repair, which is independent of its transcriptional roles (*32*). ATM has been shown to phosphorylate ATF2 on serines 490 and 498 after exposure to ionizing radiation (*32*). Phosphorylated

ATF2 foci have also been shown to co-localize with γ–H2AX and Mre11/Rad50/NBS1 foci (*32*). Inhibition of ATF2 results in a decreased recruitment of Mre11 to ionizing radiation-induced foci (IRIF), abrogates the S-phase checkpoint, reduces activation of ATM, Chk1 and Chk2, and increases cells radiosensitivity (*32*). Moreover, ATF2 may play a role in helping tumor cells to escape death, because overexpression of ATF2 has been shown to confer radioresistance to melanoma cells (*33*). A further implication for a role of ATF2 in carcinogenesis has recently been found in the lower ATF2 mRNA levels in breast cancer tissue as compared to normal breast tissue (*34*).

Structural maintenance chromosome 1 (SMC1) has also been reported to have a role in responding to ionizing radiation damage. SMC1 is phosphorylated on serine 957 by ATM in response to DSBs in an NBS-dependent manner, and co-localizes with γ–H2AX and other proteins at the sites of DSBs (*35, 36*). In cells SMC1 exists as part of the cohesin complex, which contains hSMC3, hRad21 and hSA2, as well as in a heterodimer form with only hSMC3 (*37*). Cohesin is essential for sister chromatid unity, and chromosome segregation, and plays a role in chromosome condensation (*35, 38*). In yeast, the SMC1/SMC3 heterodimer has been shown to play a role in coordinating the repair of DSBS, favoring homologous recombination (HR) over non-homologous end joining (NHEJ) when sister chromatids are available (*39*).

Our goal in this study was to determine whether we could detect discrete biological responses after low- or high-LET radiation exposures based on phospho-protein profiles. Denoting the phospho-protein kinetics may also provide a better understanding of the underlying cellular responses occurring after these exposures. To this end, we detailed the kinetics for three proteins that are functional in radiation repair

and signal transduction, γH2AX, ATF2 and SMC1 following X-ray and iron-ion exposure. The phospho-proteins chosen have been noted to be at the sites of DSB's after irradiation, to have roles in the damage response, and, in the case of SMC1 and ATF2, to be specifically phosphorylated by ATM and have a role in maintaining cell cycle blocks after damage (Fig. 1). Flow cytometry analysis was developed and optimized to more rapidly determine phospho-protein kinetics, and to identify any cell cycle-dependent differences as well. We found that the phosphorylation profiles differed depending on the radiation quality, dose, cell cycle and phospho-protein studied.

METHODS AND MATERIALS

Cell Culture

82-6 hTERT immortalized fibroblast cells (gift of Judith Campisi) were grown in DMEM (all medium and supplements from Gibco, Invitrogen, Carlsbad, CA) supplemented with 10% fetal bovine serum, antibiotic-antimycotic (1X) and L-glutamine (2mM). T-75 flasks were plated for each time and dose, and grown to 85 to 95% confluence prior to exposure. Approximately 80% (+/-10%) of the cells were in G1 at the time of irradiation for all experiments. Cells were also plated for microscopic detection of foci at the same cell density in chamber slides.

Irradiation Conditions

Cells were exposed to four doses (0.05, 0.1, 0.5 and 2 Gy) of 320 kV X-rays or 1000 MeV/nucleon iron-ions (LET of 150 keV/μm). X-ray exposures were performed at Lawrence Berkeley National Laboratory, using dose rates ranging from 5 to 80 cGy/min depending on the dose. Iron-ion exposures were performed at Brookhaven National Laboratory using dose rates ranging from 10cGy to 1 Gy/min. depending on dose.

Chamber plated for microscopic quantification of phospho-protein foci were irradiated horizontal to the beam to more accurately quantify focus numbers without necessitating confocal analysis, whereas flasks for flow cytometry were irradiated vertical to the beam, because direction does not affect accurate detection in this case. Irradiating horizontal or vertical to the beam does not affect dose calculations; doses are the same for horizontal and vertical directions because the LET is nearly constant across the samples in either direction. Both slides and flasks were irradiated at the same time and received equivalent doses. Three independent experiments for both iron ions and X rays were performed, and error bars in the figures are SE.

Antibodies

Primary antibodies used included mouse monoclonal γ–H2AX (1:800 dilution), pSMC1 Ser^{957} (1:800 dilution) from Upstate (Lake Placid, NY), and rabbit polyclonal pATF2 $Ser^{490/498}$ (1:1000 dilution) from Rockland (Gilbertsville, PA). Secondary antibodies were from Molecular Probes, Invitrogen (Carlsbad, CA), goat anti-mouse 488, and goat anti-rabbit 488 (both used at 1:400 dilution), and were used with each of the appropriate primary antibodies. Cell cycle status was determined by staining cellular DNA with propidium iodide (PI, Roche Applied Science, Indianapolis, IN), at a final concentration of 10 μg/ml. RNAse A was obtained from Sigma-Aldrich (St.Louis, MO) and used at a final concentration of 100 μg/ml.

Fixation and staining for Flow cytometry analysis

Flasks or chamber slides were fixed at various times (0.5, 2, 4, 8 and 24 h) after each dose; a control was also fixed at each of these times. A methanol fixation was optimized for use for γ–H2AX and pSMC1 Ser^{957}, and a paraformaldehyde fixation followed by a

subsequent methanol fixation was used for pATF2 $Ser^{490/498}$. After fixation, cells were placed at -20° C until they were stained. Cells suspensions were counted prior to staining and diluted to 1.0 x 10^6 /ml. For staining, an aliquot of the fixed cells containing 0.5 to 1.0 x 10^6 of cells was removed and washed in PBS. Cells were then placed in a blocking solution containing 2% FBS/PBS and incubated for 1 h in primary antibody on ice. After incubation, cells were pelleted and washed in PBS, than incubated in a secondary antibody diluted in blocking solution. After 1 h additional incubation on ice under foil, cells were pelleted and washed for a final time in PBS. Cells were then resuspended in PBS containing PI and RNase, or in RNase alone to serve as a control for any spectral overlap of Molecular Probes 488 and PI.

Flow cytometry Analysis

Median values of fluorescent signals corresponding to the phosphorylation levels of the noted proteins were obtained for each sample and unirradiated control for three independent experiments for each radiation quality. Data are expressed as the relative increase in phosphorylation level over controls for each independent staining, this allows for normalization of the data and for comparisons of samples stained on different days and analyzed using different machines. In some cases, data are presented as the percentage of that maximally induced, using the dose and time at which maximal induction occurred as 100%.

Fixation and Staining for Microscopic Analysis

Chamber slides were seeded at the same density as the flasks for flow cytometry analysis and were fixed at the same times using the same fixation and staining procedures. Slides were coded and scored blindly in all cases. For studies detailing γ–H2AX foci, 100 cells

for each control, dose and time from one representative iron-ion experiment were scored. At early time points when tracks were present, individual foci constituting tracks were counted when visually resolvable. The background levels of γ–H2AX foci in control cells ranged from 0.4 to 0.5 foci/cell depending on the time point. For pATF2 $Ser^{490/498}$ and pSMC1 Ser^{957} foci over 100 cells were scored blindly for number of foci per cell as well as the number of cells containing foci for each control and radiation quality 2h after irradiation with 0.5 Gy (See Table 1). Background levels of pATF2 $Ser^{490/498}$ and pSMC1 Ser^{957} foci were similar for both X-ray and Fe experimental control samples (both phospho-proteins showed less than 0.3 foci/cell).

RESULTS

Optimization of Flow-based Quantification of Phospho-protein Levels

Initial studies were performed to identify specificity of the antibodies, optimal fixation methods, and staining conditions for flow cytometry-based detection of each phospho-protein. Specificity of antibodies was also confirmed by Western blot analyses (results not shown).

Relationship between Total Fluorescence Levels and Radiation-induced Foci after Iron-ion Exposure

Previous studies have documented a similar dose-response relationship between total γ–H2AX fluorescence levels and foci numbers after low-LET radiation exposures (*40*). However, a similar relationship cannot be assumed after high-LET radiation

exposure because of the differences in energy deposition and track structure. Therefore, foci were scored and total fluorescence quantified for one representative study to determine whether a similar dose-response relationship between total fluorescence and focus number existed for high-LET radiation (Fig. 2). Values are given as percentages of the maximal values for both total fluorescence levels as detected by flow cytometry and number of foci scored microscopically to allow comparisons between the methods. When comparing the endpoints for all doses and times, a similar linear relationship between numbers of foci and the level of total fluorescence is observed. At early times after exposure (0.5 and 2 h, Fig. 2A and B) focus numbers are lower compared to the total fluorescence levels. This likely reflects the fact that samples were irradiated horizontal to the beam so that tracks are formed in the cells, and individual foci which make up tracks are difficult to resolve at early times after exposure, whereas flow cytometry measures total fluorescence levels, so track structure does not hinder quantification at early times. However, a few hours post exposure when tracks begin to resolve into individual foci and can be determined more easily, a good agreement between the methods is obtained, with 4 h after exposure showing the closest match (Fig 2C).

Comparison of Phospho-protein Induction Using Flow Cytometry Analysis

Iron-ion exposure resulted in a greater induction and persistence of γ–H2AX per unit dose than X rays (Fig. 3A and D). Lower doses of iron ion ($\leq$ 0.5 Gy) on average did not reach maximal levels of γ–H2AX until 2 h after exposure (Fig. 4D), whereas the highest dose of 2 Gy reached maximal induction levels at 0.5 h post irradiation (Fig. 3D). This delay in reaching maximal levels of phosphorylation after exposure was not

exhibited with X rays, where maximal γ–H2AX inductions were obtained at 0.5h after irradiation at all doses and persisted at this level for up to 2h after exposure (Fig. 3A and 4A). Taken together, these data suggest that both dose and radiation quality affect the γ–H2AX kinetics.

pATF2 $Ser^{490/498}$ (referred to herein as pATF2) showed lower total levels of phosphorylation after iron-ion compared to X-ray exposure at all the doses studied (Fig. 3 B and E). Although total fluorescence levels indicated a very clear difference when radiation qualities were compared, these differences could be due to a number of factors. For example, fewer phospho-protein-positive cells, fewer foci per cell, or some combination of these could all lead to lower total fluorescence levels. To distinguish between these possibilities, foci were imaged and scored blindly for each quality of radiation at a single dose and time at which a clear difference in total fluorescence was noted. Scoring pATF2 foci 2h post 0.5 Gy revealed that the lower total fluorescence level exhibited in iron-ion exposed cells was likely due to a combination of both fewer foci per cell and fewer focus-positive cells (Table 1, Fig. 5). Control values were similar for both X-ray- and iron-ion exposed cells, ranging from 84-93% and 93-97% of the cells without foci, and 0.3 and 0.1 focus per cell in control iron ion and X-ray experiments, respectively (Table 1). In images of radiation-induced pATF2 foci, it also appears that there may be differences in focus size after iron-ion and X-ray exposure, with X-ray exposure resulting in slightly larger foci. Therefore lower total ATF2 phosphorylation in iron-ion exposed cells as measured by flow cytometry is reflected at the microscope level as fewer focus-positive cells, fewer foci per cell, and smaller foci.

pSMC1 Ser^{957} (referred to herein as pSMC1) shows a lower induction after iron-ion compared to X-ray exposure, particularly at the highest dose (Fig. 3C and F), however this difference is not significant. Images of pSMC1 radiation induced foci also reveals that slight differences in total phosphorylation levels likely reflect the fact that iron-ion exposed cells contain fewer foci per cell and fewer focus-positive cells (Table 1 and Fig 5). After the highest dose of X-rays (2 Gy), maximal levels were obtained at the earliest time and showed a gradual decline over time (Fig. 7A). In contrast, after a 2 Gy dose of iron-ions, levels were at a low maximal level at the earliest time and remained at these levels up to 24 h after exposure (Fig. 7C). However, with both qualities of radiation at doses below 2 Gy, pSMC1 consistently showed a delay in reaching maximal phosphorylation levels, reaching maximal levels at 2 h after X irradiation and 4 h after iron-ion exposure (compare times of pSMC1 peaks in Fig. 3C vs F, and Fig. 4C and F). Taken together, these results support unique differences in pSMC1 profiles that depend on the dose and radiation quality.

When the phosphorylation profiles over time for all three phospho-proteins were compared in area graphs, particular patterns were noted based on the phospho-protein, dose and radiation quality. Following a 2 Gy dose of X-ray, induction levels for all three phospho-proteins appear much more similar than what is observed following a 2 Gy dose of Fe nuclei, where levels of pSMC1 and pATF2 are approximately one-forth of the levels of γH2AX (Fig. 7 A and C). After a 2 Gy dose of both X-rays and iron-ions, γ–H2AX shows a quicker resolution than the other two ATM-dependent phospho-proteins, which are more persistent, especially after high-LET exposures. After a 0.5 Gy dose, differences are again noted based on radiation quality. Following X irradiation,

γ–H2AX levels are much lower than either pATF2 or pSMC1, whereas after iron-ion exposure, levels of all three are much more similar (Fig. 7B and D). In fact, for all lower doses (0.05 to 0.5 Gy) of low-LET radiation (Fig. 7B, 8A and B), pATF2 and pSMC1 levels are always higher than γ-H2AX levels, but a different pattern is observed after the same doses of high-LET radiation. pATF2 shows a lower or at best an equal level of phosphorylation compared to γ–H2AX levels at all lower doses (0.05 to 0.5 Gy) and times after iron-ion irradiation. pSMC1, however, shows a more comparable level of phosphorylation to levels of γ–H2AX at lower doses of iron-ions, and thus is more similar to the levels induced by X-rays in this dose range, although its maximal level of expression is later after exposure to high-LET (4 h after iron ion exposure compared to 2 h after X-ray exposure). These results point to distinct temporal patterns of phosphorylation that depend on radiation quality and phospho-protein.

Comparisons of pATF2 and γH2AX Fluorescence Levels on an Individual Cell Basis after Iron-ion and X-ray Exposure

Data for individual G1 cells was exported using FlowJo software (Tree Star, Inc.) for pATF2 and γ–H2AX, 0.5 h after 2 Gy irradiation. The percentages of cells showing various relative increases over the control levels are plotted for each phospho-protein in Fig. 6. After X-ray exposure (Fig. 6A), the percentage of cells with various levels of damage (as approximated by γ–H2AX levels) corresponds well with the induction of pATF levels. In contrast, iron-ion exposure results in higher γ–H2AX levels (i.e. damage) but the levels of pATF2 are not correspondingly high (Fig. 6B). These data

reveal that induced ATF2 phospho-protein levels are dependent on the radiation quality.

Comparison of Phospho-Protein Kinetics in Different Phases of the Cell Cycle

The kinetics of phosphorylation after a 2 Gy dose of iron-ion or X-ray was compared for each phospho-protein in each phase of the cell cycle (Fig. 9). The values shown are the percentage of maximal phosphorylation remaining after subtracting control levels, and for each cell cycle, control levels for that cell cycle were used. This analysis reveals distinct differences in the percentage of γ–H2AX remaining at different times after exposure that are dependent on the cell cycle. In G_1 phase, higher γ–H2AX levels were observed at the earliest time compared to other cell cycles, and G_1-phase cells remained phosphorylated longer compared to other phases of the cell cycle as well. In contrast, pATF2 and pSMC1 phosphorylation levels appeared to be much more similar between different phases of the cell cycle after both iron-ion and X-ray exposures. In addition, a striking persistence in phosphorylation is also observed after high-LET radiation exposures compared to low-LET radiation exposures when comparing residual levels of pATF2 and pSMC1 at 24 h after exposure.

DISCUSSION

All of the phospho-proteins studied in the current work have been documented to be functional in the DNA damage response and to co-localize at the sites of DSB's after ionizing radiation; thus we might expect fairly similar phospho-protein profiles. However, unique phospho-protein profiles were identified based on the radiation quality, the specific phospho-protein, the dose, the time, and cell cycle.

Initial studies were performed measure radiation-induced foci (IRIF) and total fluorescence levels as detected by flow cytometry for γ–H2AX, and the results were compared to determine whether a similar relationship between focus numbers and total fluorescence levels existed after iron-ion exposure. Our studies indicated that levels of γ–H2AX foci and total fluorescence showed similar dose-dependent relationships. Previous studies have noted a good correspondence between focus numbers and numbers of DSBs at earlier times after exposure (*25, 26*), and our current study indicates that total fluorescence levels should also provide an accurate indicator of relative levels of DSBs after iron-ion exposure.

As expected based on previous studies (*41, 42*), a greater persistence and induction of γ–H2AX was observed after high-LET radiation exposures. An RBE of 1.8 was determined at 0.5 h after exposure using the average median γ–H2AX values for X-rays and iron-ions from our studies. This RBE is identical to the RBE calculated for iron-ions using detailed PFGE studies (*14*). Our studies also reveal that at lower doses of iron-ions (≤0.5 Gy), but not X-rays, γ–H2AX levels continue to increase up to 2 h after exposure. Since the γ–H2AX levels after exposure to iron-ions and X-rays at the earliest time (0.5 h) relate well to the RBE based on DSBs induced after these exposures, the increased fluorescence at later times may reflect γ–H2AX occurring downstream of the initial sites. An increase in focus size in high-LET radiation exposed cells that was not observed after low-LET radiation exposure has been noted previously in studies comparing nitrogen-ion and X-ray induced foci (*43*). These researchers also concluded that this effect was likely due to additional γ–H2AX phosphorylation occurring downstream of the initial damage site.

In comparisons of radiation quality-dependent pSMC1 profiles, a maximal level of phosphorylation was observed 4 h after iron-ion exposure and 2 h after X-ray exposure at all doses < 2 Gy. In contrast, pATF2 reached maximal levels at the earliest time studied. Both ATF2 and SMC1 have been reported to have a role in maintaining an S-phase block after DNA damage (*32, 35*). The observed early pATF2 induction and delayed maximal induction in pSMC1 may imply that SMC1 serves as a backup for ATF2 at later times after damage when there is still a need to block replication before repair has been completed. This delay in repairing damage would be expected to be longer after iron-ion exposure than after X-ray exposure, because we know from previous work that high-LET particles produce more closely spaced and complex types of breaks that are likely more difficult to repair (*15, 16*). A consistent pattern of peak pSMC1 expression (4 h post exposure) occurring at a time following peak γH2AX levels (2 h post exposure) is evident when examining phospho-protein relationships after low doses of iron-ions (Fig. 7D and Fig. 8C & D). These results suggest that SMC1 may play a role in the final resolution of remaining DSBs. In yeast, a role for SMC1 has also been described for facilitating HR repair over NHEJ when a sister homolog is present (*39*); thus this delayed peak in pSMC1 levels could also reflect a time at which this function is at its highest. Further studies would be needed to establish which, or whether both of these roles leads to these observed pSMC1 kinetics.

A unique capability of flow-based studies is their ability to determine cell cycle status in addition to one or more other protein profiles. When comparing the phospho-profiles based on cell cycle, we see unique differences in the phospho-kinetics for these proteins. For instance, in G_1, γ–H2AX appears to be induced to a greater extent than in

other phases of the cell cycle after control levels are subtracted. This could imply either that cells in S and G_2 do not induce as much γ–H2AX after damage or that the majority of repair takes place very quickly (by 0.5h post irradiation when the first fixation was performed) in these cell cycles compared to G_1. Previous studies have noted that the cell is more resistant to damage in S phase (*44*) and that repair is more rapid in G_2 due to a backup repair pathway which is more enhanced in G_2 (*45*). Both of these findings may explain the reduced induction and more rapid resolution of γ–H2AX in G_2 and S phases of the cell cycle. Another study using flow cytometry analysis also noted a greater γ–H2AX induction after irradiation in G_1 than in S-phase and concluded that this was due to the higher background levels of γ–H2AX in S phase cells (*40*). Interestingly, neither pSMC1 nor pATF2 showed a difference in kinetics based on cell cycle. The fact that no radiation-induced cell cycle-dependent differences in phosphorylation patterns were noted for these latter proteins was somewhat unexpected given that both pATF2 and pSMC1 are known to have a role in maintaining S-phase block after damage, and it might be expected that more S-phase cells would therefore be phosphorylated. However, the data indicate that these proteins are phosphorylated at fairly similar levels in all phases of the cell cycle, perhaps implying an important DNA damage response role for these proteins in G_1 and G_2 phases as well.

The lower inductions of phosphorylation for the two ATM-mediated proteins after exposure to 2 Gy of iron-ions as compared to X-rays is especially unusual given the high levels of γ–H2AX induced by iron-ions and the previous DSB studies indicating that iron-ions induce more damage (*14*). Although similar trends were observed for both of the ATM-mediated phosphorylations, pSMC1 showed a less dramatic difference between

radiation qualities at lower doses. This is likely due to technical reasons related to non-specific background levels of fluorescence with this anti-body that make it more challenging to detect significant differences in total fluorescence by flow cytometry. This is supported by the fact that our focus studies clearly show significant differences in phosphorylation levels for pSMC1 as well as pATF2, with both proteins showing lower levels of phosphorylation after iron-ion exposure than after X-ray exposure (Table 1 and Fig. 5). Given that both pATF2 and pSMC1 are phosphorylated in a solely ATM-dependent manner, the lower phosphorylation levels observed after iron-ion exposure may imply that ATM has more difficulty recognizing and responding to high-LET radiation damage deposited in such a close and clustered manner within a cell.

It is also realized that not all cells within the population will be hit by the primary ion track at the lowest doses of iron-ion used here (0.05 and 0.1 Gy); however, studies indicate that δ rays from the primary track should expose all the cells in the population to a dose, albeit a low dose. Delta rays produce a low-LET form of radiation very similar to that of X-rays, since both are induced by single electron tracks; however, doses from δ rays will vary greatly depending on their distance from the primary track and their energy (*19, 46*). Modeling studies have determined that the average dose for cells exposed only to δ rays in this current work would be 0.015 Gy and 0.05 Gy after exposure to 0.05 and 0.1 Gy iron-ions, respectively (personal communication from F. Cucinotta). Therefore, the low-LET δ ray dose in cells exposed to 0.1 Gy of iron-ions should on average be equivalent to a 0.05 Gy dose of X-rays. When comparing total fluorescence levels for 0.1 Gy of ion-ions to 0.05 Gy of X-rays, we do note similar pATF2 levels. This implies that cells receiving a similar dose of δ rays may induce a similar level of pATF2. However,

when all cells are exposed to the direct track as with a 0.5 and 2 Gy dose, it appears that the high-LET portion of the dose does not induce levels of phosphorylation equal to those induced by similar X-ray doses. We hypothesized that perhaps the heavily damaged iron-ion exposed cells may not be initiating ATF2 (or SMC1) phosphorylation, thus explaining the higher numbers of cells that contain no pATF2 and pSMC1 foci after iron-ion exposure. To determine whether this was the case, we compared fold inductions of pATF2 and γH2AX 0.5 h after exposure to a 2 Gy of iron-ions or X-rays. We observed similar percentages of cells showing similar fold inductions in pATF2 or γH2AX after X irradiation, but we noted a lack of high-fluorescing pATF2 cells after the iron-ion exposure, even though heavily damaged cells were present as indicated by the relative inductions of γ–H2AX. These data suggest that the heavily damaged iron-ion exposed cells do not induce ATF2 phosphorylation. It is also striking that these two ATM phosphorylated proteins appear to be phosphorylated much more persistently after iron-ion exposure than after X irradiation in all phases of the cell cycle. Thus ATM-mediated phosphorylation kinetics and amplitude appear to be influenced by radiation quality.

Our results confirm that biological responses resulting from exposure to radiations of different quality can be differentiated based on phospho-protein profiles. However, cell cycle and dose are important factors to consider when analyzing data. A role for ATM in regulating the levels of phosphorylation of downstream proteins based on radiation quality is also consistent with our results. Finally, this study highlights the power of flow cytometry in comparing multiple phospho-proteins patterns in a cell cycle-dependent manner in individual cells to better understand differences between radiation

qualities and dose, and has revealed that it may be harnessed to better understand the DNA damage response.

ACKNOWLEDGEMENTS

I would like to thank Drs Aloke Chatterjee, Frank Cucinotta, Bjorn Rydberg and Steve Yannone for their thoughtful review and helpful comments. We gratefully acknowledge financial support provided by NASA (03-OBPR-07-0032-0027). This work was supported by the Director, Office of Science, Office of Basic Energy Sciences, of the U.S. Department of Energy under Contract No. DE-AC02-05CH11231. We would also like to recognize the help and support of Hector Nolla as part of the UC Berkeley Flow Cytometry Core.

TABLE 1
Comparison of Ionizing Radiation Induced pATF2 and pSMC1 Foci
2 Hours Post a 0.5 Gy Dose of Xray or Fe Nuclei

Phospho-protein	Radiation Type	Number of Cells Scored	Average Number of Foci/Cell	Number of Cells not Containing Foci (%)
pATF2	Xray	147	2.4	19 (13%)
	Control[a]	199	0.08	185 (93%)
	Fe nuclei	155	1.3	80 (52%)
	Control[b]	229	0.13	213 (93%)
pSMC1	Xray	174	4.0	18 (10%)
	Control[a]	171	0.27	143 (84%)
	Fe nuclei	179	0.5	120 (67%)
	Control[b]	191	0.17	186 (97%)

[a] Control was set up at same time and mock irradiated at time of Xray experiment
[b] Control was set up at same time and mock irradiated at time of Fe experiment

Figure Legends

Figure 1:

Radiation induces DSBs that then initiate a complex cascade of phosphorylations. Phosphorylations on these proteins are important in the resolution and repair of DNA damage after irradiation. The phospho-proteins studied are shown in white ovals, proteins involved in phosphorylation of these proteins are shown in gray shaped figures, and the processes the proteins are believed to play a role in are in boxes. Phosphorylation of H2AX on Ser 139 is mediated by ATM, ATR and DNA-PKcs. ATM-dependent phosphorylations occur on ATF2 and SMC1 at Ser 490/498 and Ser 957, respectively. pATF2 and pSMC1 are proposed to have roles both in DNA repair and maintaining S-phase block after damage. The star symbols (❋) represent phosphorylations occurring on these proteins, and arrows indicate proteins involved in phosphorylating these proteins. ATF2 has also been shown to have a role in increasing activation of ATM after damage; thus the dual arrow between these proteins.

Figure 2:

Comparison between the number of γH2AX foci detected microscopically and flow-cytometry-detected total phosphorylation levels after iron-ion exposure. To allow comparison between these methods, data are presented as a percentage of maximally induced levels; and for both data sets, maximal induction occurs 2 h after 2 Gy. Bars represent the percentage of maximal foci induced, and the data points represent the percentage of maximal total fluorescence induced. Data shown are for one representative

iron-ion experiment for doses of 0.05, 0.1, 0.5 and and 2 Gy, 0.5 h (panel A), 2 h (panel B), and 4 h (panel C) after exposures.

Figure 3:

Comparison of phospho-protein profiles after exposure of cells to X-rays and iron-ions using flow cytometry. Median values of total fluorescence were obtained for each dose and time. Average median values from three independent experiments are plotted relative to the control for both X-rays (top panels) and iron-ions (lower panels), with error bars representing standard errors. Each time is represented by a different symbol and color (blue ♦=0.5h, red ■= 2h, green ▲ =4h, aqua ✕= 8h, purple ○ = 24h). The kinetics of γ–H2AX (panel A), pATF2 (panel B) and pSMC1 (panel C) after X-ray exposure and Fe Ion (E), and γ–H2AX (panel D), pATF2 (panel E) and pSMC1 (panel F) levels following iron-ion exposure are shown.

Figure 4:

Comparison of phospho-protein profiles after exposure of cells to low doses (0.05 to 0.5 Gy) of X-rays and iron-ions using flow cytometry. Data are shown only in this lower dose range for each to better exhibit differences. Median values are plotted relative to the control levels for both X-rays and iron-ions, and error bars represent standard errors. Data are from three independent iron-ion and X-ray experiments. Each time is represented by a different symbol and color (blue ♦=0.5h, red ■= 2h, green ▲ =4h, aqua ✕= 8h, purple ○ = 24h). The kinetics of γ–H2AX (panel A), pATF2 (panel B), and

pSMC1 (panel C) after X-ray exposure and γ–H2AX (panel D), pATF2 (panel E), and pSMC1 (panel F) after iron-ion exposure are shown.

Figure 5:

Comparison of radiation-induced γ–H2AX (panels A and D), pATF2 (panels B and E) and pSMC1 (panels C and F) foci from a representative X-ray (top panels) and iron-ion (lower panels) experiment. Images of microscopic foci detected 2 h after a 0.5 Gy exposure are shown. Each phospho-site antibody was indirectly labeled with Molecular Probes 488 secondary antibody (green), and cells were counterstained with DAPI (blue). All images were taken with the same exposure times. White ovals outline the DAPI-stained cells within each field that do not contain foci.

Figure 6:

The percentages of cells showing various increases in phosphorylation over control levels of γ–H2AX (black bars) and pATF2 (white bars) after X-ray (panel A) and iron-ion (panel B) exposure. Error bars represent standard errors from three independent X-ray or iron-ion experiments.

Figure 7:

Comparison of the fluorescence levels of each phospho-protein at various times after X-ray (top panels) or iron-ion (lower panels) exposure. γ–H2AX phosphorylation levels are shown in dark blue, pATF2 in green, and pSMC1 in aqua. Levels are shown after a

dose of 2 Gy (panels A, C) and 0.5 Gy (panels B,D) of X-rays or iron-ions. Data are shown as relative fluorescence for three independent iron-ion and X-ray experiments.

Figure 8:

Comparison of the total fluorescence levels for each phospho-protein at various times after X-ray (top panels) or iron-ion (lower panels) exposure. γ–H2AX phosphorylation levels are shown in dark blue, pATF2 in green, and pSMC1 in aqua. Levels are shown after a dose of 0.1 Gy (panels A, C) and 0.05 Gy (panels B, D) of X-rays or iron-ions. Data are shown as relative fluorescence for three independent iron-ion and X-ray experiments.

Figure 9:

The relationship between phospho-protein kinetics and cell cycle. Bars show the percentage of induced phosphorylation remaining in G1 (panels A & D), S (panels B & E) or G2 (panels C & F) phases of the cell cycle after a 2 Gy dose of X-rays (top panels) or iron ions (lower panels). Levels of phosphorylated γ–H2AX (black bar), pATF2 (white bar), and pSMC1 (gray bar) are shown. Bars represent standard errors for three independent iron-ion and X-ray experiments.

REFERENCES

1. P. L. Olive, The role of DNA single- and double-strand breaks in cell killing by ionizing radiation. *Radiat Res* **150**, S42-51 (1998).

2. K. M. Prise, M. Pinto, H. C. Newman and B. D. Michael, A review of studies of ionizing radiation-induced double-strand break clustering. *Radiat Res* **156**, 572-576 (2001).

3. J. D. Friesner, B. Liu, K. Culligan and A. B. Britt, Ionizing radiation-dependent gamma-H2AX focus formation requires ataxia telangiectasia mutated and ataxia telangiectasia mutated and Rad3-related. *Mol Biol Cell* **16**, 2566-2576 (2005).

4. E. J. Park, D. W. Chan, J. H. Park, M. A. Oettinger and J. Kwon, DNA-PK is activated by nucleosomes and phosphorylates H2AX within the nucleosomes in an acetylation-dependent manner. *Nucleic Acids Res* **31**, 6819-6827 (2003).

5. I. M. Ward and J. Chen, Histone H2AX is phosphorylated in an ATR-dependent manner in response to replicational stress. *J Biol Chem* **276**, 47759-47762 (2001).

6. T. Stiff, M. O'Driscoll, N. Rief, K. Iwabuchi, M. Lobrich and P. A. Jeggo, ATM and DNA-PK function redundantly to phosphorylate H2AX after exposure to ionizing radiation. *Cancer Res* **64**, 2390-2396 (2004).

7. S. E. Golding, E. Rosenberg, A. Khalil, A. McEwen, M. Holmes, S. Neill, L. F. Povirk and K. Valerie, Double strand break repair by homologous recombination is regulated by cell cycle-independent signaling via ATM in human glioma cells. *J Biol Chem* **279**, 15402-15410 (2004).

8. D. A. Dart, K. E. Adams, I. Akerman and N. D. Lakin, Recruitment of the cell cycle checkpoint kinase ATR to chromatin during S-phase. *J Biol Chem* **279**, 16433-16440 (2004).

9. P. A. Jeggo, DNA breakage and repair. *Adv Genet* **38**, 185-218 (1998).

10. D. W. Chan, B. P. Chen, S. Prithivirajsingh, A. Kurimasa, M. D. Story, J. Qin and D. J. Chen, Autophosphorylation of the DNA-dependent protein kinase catalytic subunit is required for rejoining of DNA double-strand breaks. *Genes Dev* **16**, 2333-2338 (2002).

11. K. M. Prise, M. Folkard, H. C. Newman and B. D. Michael, Effect of radiation quality on lesion complexity in cellular DNA. *Int J Radiat Biol* **66**, 537-542 (1994).

12. A. Ottolenghi, M. Merzagora and H. G. Paretzke, DNA complex lesions induced by protons and alpha-particles: track structure characteristics determining linear energy transfer and particle type dependence. *Radiat Environ Biophys* **36**, 97-103 (1997).

13. W. Burkart, T. Jung and G. Frasch, Damage pattern as a function of radiation quality and other factors. *C R Acad Sci III* **322**, 89-101 (1999).

14. M. Lobrich, P. K. Cooper and B. Rydberg, Non-random distribution of DNA double-strand breaks induced by particle irradiation. *Int J Radiat Biol* **70**, 493-503 (1996).

15. K. M. Prise, Use of radiation quality as a probe for DNA lesion complexity. *Int J Radiat Biol* **65**, 43-48 (1994).

16. T. J. Jenner, C. M. deLara, P. O'Neill and D. L. Stevens, Induction and rejoining of DNA double-strand breaks in V79-4 mammalian cells following gamma- and alpha-irradiation. *Int J Radiat Biol* **64**, 265-273 (1993).

17. S. Kozubek and E. A. Krasavin, Cell sensitivity to irradiation and DNA repair processes. II. The cell sensitivity to ionizing radiation of different LETs. *Neoplasma* **31**, 685-695 (1984).
18. R. Katz and M. N. Varma, Radial distribution of dose. *Basic Life Sci* **58**, 163-179; discussion 179-180 (1991).
19. F. A. Cucinotta, H. Nikjoo and D. T. Goodhead, The effects of delta rays on the number of particle-track traversals per cell in laboratory and space exposures. *Radiat Res* **150**, 115-119 (1998).
20. F. A. Cucinotta, W. Schimmerling, J. W. Wilson, L. E. Peterson, G. D. Badhwar, P. B. Saganti and J. F. Dicello, Space radiation cancer risks and uncertainties for Mars missions. *Radiat Res* **156**, 682-688 (2001).
21. H. Wu, M. Durante, K. George and T. C. Yang, Induction of chromosome aberrations in human cells by charged particles. *Radiat Res* **148**, S102-107 (1997).
22. K. M. Prise, G. Ahnstrom, M. Belli, J. Carlsson, D. Frankenberg, J. Kiefer, M. Lobrich, B. D. Michael, J. Nygren, et al., A review of dsb induction data for varying quality radiations. *Int J Radiat Biol* **74**, 173-184 (1998).
23. E. P. Rogakou, D. R. Pilch, A. H. Orr, V. S. Ivanova and W. M. Bonner, DNA double-stranded breaks induce histone H2AX phosphorylation on serine 139. *J Biol Chem* **273**, 5858-5868 (1998).
24. E. P. Rogakou, C. Boon, C. Redon and W. M. Bonner, Megabase chromatin domains involved in DNA double-strand breaks in vivo. *J Cell Biol* **146**, 905-916 (1999).
25. O. A. Sedelnikova, E. P. Rogakou, I. G. Panyutin and W. M. Bonner, Quantitative detection of (125)IdU-induced DNA double-strand breaks with gamma-H2AX antibody. *Radiat Res* **158**, 486-492 (2002).
26. K. Rothkamm and M. Lobrich, Evidence for a lack of DNA double-strand break repair in human cells exposed to very low x-ray doses. *Proc Natl Acad Sci U S A* **100**, 5057-5062 (2003).
27. T. Tanaka, M. Kajstura, H. D. Halicka, F. Traganos and Z. Darzynkiewicz, Constitutive histone H2AX phosphorylation and ATM activation are strongly amplified during mitogenic stimulation of lymphocytes. *Cell Prolif* **40**, 1-13 (2007).
28. H. T. Chen, A. Bhandoola, M. J. Difilippantonio, J. Zhu, M. J. Brown, X. Tai, E. P. Rogakou, T. M. Brotz, W. M. Bonner, et al., Response to RAG-mediated VDJ cleavage by NBS1 and gamma-H2AX. *Science* **290**, 1962-1965 (2000).
29. M. Suzuki, K. Suzuki, S. Kodama and M. Watanabe, Phosphorylated histone H2AX foci persist on rejoined mitotic chromosomes in normal human diploid cells exposed to ionizing radiation. *Radiat Res* **165**, 269-276 (2006).
30. S. Y. Fuchs, I. Tappin and Z. Ronai, Stability of the ATF2 transcription factor is regulated by phosphorylation and dephosphorylation. *J Biol Chem* **275**, 12560-12564 (2000).
31. D. L. Crowe and B. Shemirani, The transcription factor ATF-2 inhibits extracellular signal regulated kinase expression and proliferation of human cancer cells. *Anticancer Res* **20**, 2945-2949 (2000).
32. A. Bhoumik, S. Takahashi, W. Breitweiser, Y. Shiloh, N. Jones and Z. Ronai, ATM-dependent phosphorylation of ATF2 is required for the DNA damage response. *Mol Cell* **18**, 577-587 (2005).

33. Z. Ronai, Y. M. Yang, S. Y. Fuchs, V. Adler, M. Sardana and M. Herlyn, ATF2 confers radiation resistance to human melanoma cells. *Oncogene* **16**, 523-531 (1998).
34. T. Maekawa, T. Shinagawa, Y. Sano, T. Sakuma, S. Nomura, K. Nagasaki, Y. Miki, F. Saito-Ohara, J. Inazawa, et al., Reduced levels of ATF-2 predispose mice to mammary tumors. *Mol Cell Biol* **27**, 1730-1744 (2007).
35. S. T. Kim, B. Xu and M. B. Kastan, Involvement of the cohesin protein, Smc1, in Atm-dependent and independent responses to DNA damage. *Genes Dev* **16**, 560-570 (2002).
36. R. Kitagawa, C. J. Bakkenist, P. J. McKinnon and M. B. Kastan, Phosphorylation of SMC1 is a critical downstream event in the ATM-NBS1-BRCA1 pathway. *Genes Dev* **18**, 1423-1438 (2004).
37. A. R. Lehmann, The role of SMC proteins in the responses to DNA damage. *DNA Repair (Amst)* **4**, 309-314 (2005).
38. J. S. Kim, T. B. Krasieva, V. LaMorte, A. M. Taylor and K. Yokomori, Specific recruitment of human cohesin to laser-induced DNA damage. *J Biol Chem* **277**, 45149-45153 (2002).
39. P. Schar, M. Fasi and R. Jessberger, SMC1 coordinates DNA double-strand break repair pathways. *Nucleic Acids Res* **32**, 3921-3929 (2004).
40. S. H. MacPhail, J. P. Banath, Y. Yu, E. Chu and P. L. Olive, Cell cycle-dependent expression of phosphorylated histone H2AX: reduced expression in unirradiated but not X-irradiated G1-phase cells. *Radiat Res* **159**, 759-767 (2003).
41. K. H. Karlsson and B. Stenerlow, Focus formation of DNA repair proteins in normal and repair-deficient cells irradiated with high-LET ions. *Radiat Res* **161**, 517-527 (2004).
42. E. L. Leatherbarrow, J. V. Harper, F. A. Cucinotta and P. O'Neill, Induction and quantification of gamma-H2AX foci following low and high LET-irradiation. *Int J Radiat Biol* **82**, 111-118 (2006).
43. S. V. Costes, A. Boissiere, S. Ravani, R. Romano, B. Parvin and M. H. Barcellos-Hoff, Imaging features that discriminate between foci induced by high- and low-LET radiation in human fibroblasts. *Radiat Res* **165**, 505-515 (2006).
44. G. E. Iliakis and R. Okayasu, Radiosensitivity throughout the cell cycle and repair of potentially lethal damage and DNA double-strand breaks in an X-ray-sensitive CHO mutant. *Int J Radiat Biol* **57**, 1195-1211 (1990).
45. W. Wu, M. Wang, S. K. Singh, T. Mussfeldt and G. Iliakis, Repair of radiation induced DNA double strand breaks by backup NHEJ is enhanced in G2. *DNA Repair (Amst)* **7**, 329-338 (2008).
46. D. T. Goodhead, Initial events in the cellular effects of ionizing radiations: clustered damage in DNA. *Int J Radiat Biol* **65**, 7-17 (1994).

Figure 1

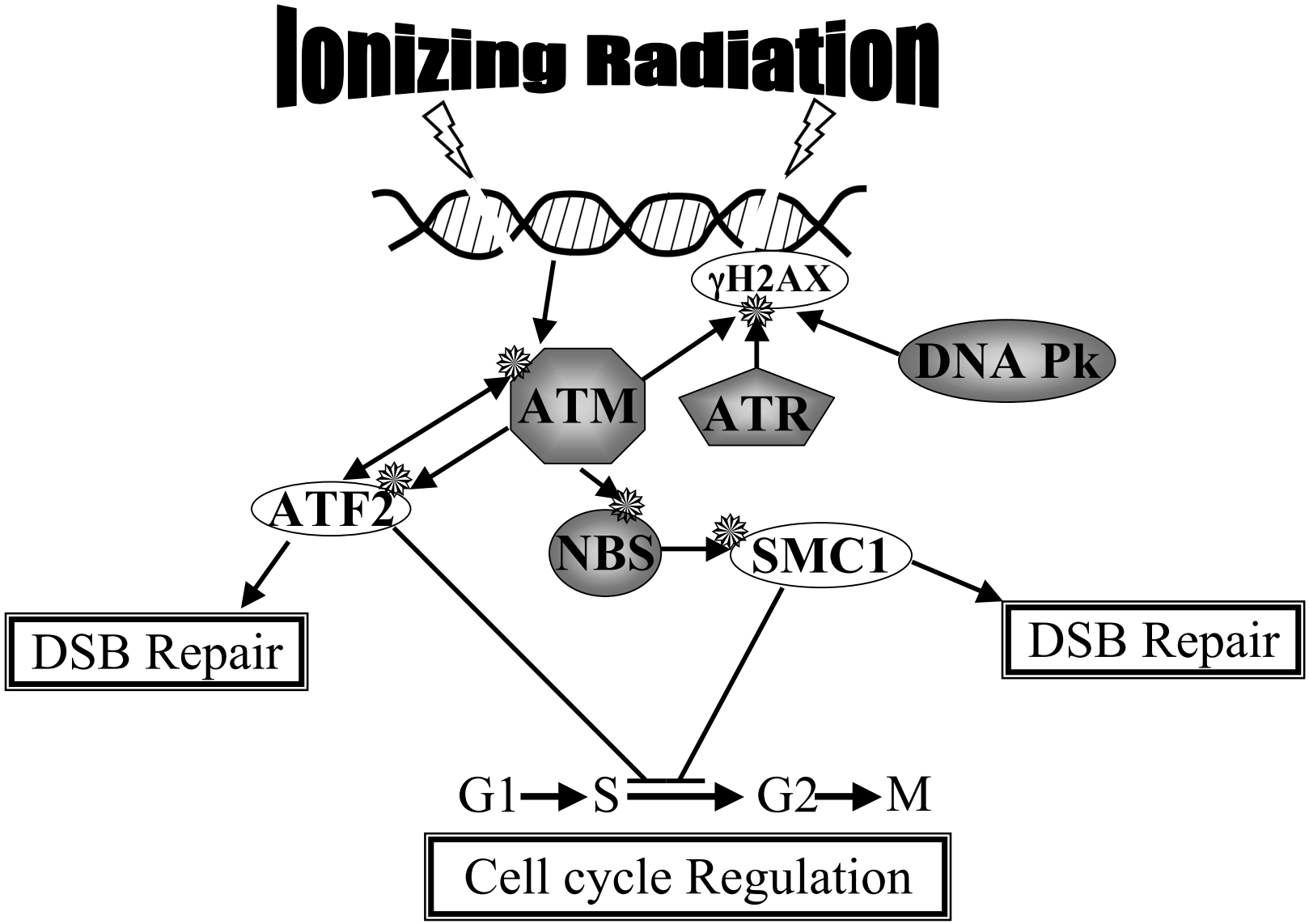
Ionizing Radiation
γH2AX
DNA Pk
ATM
ATR
ATF2
NBS
SMC1
DSB Repair
DSB Repair
G1
S
G2
M
Cell cycle Regulation

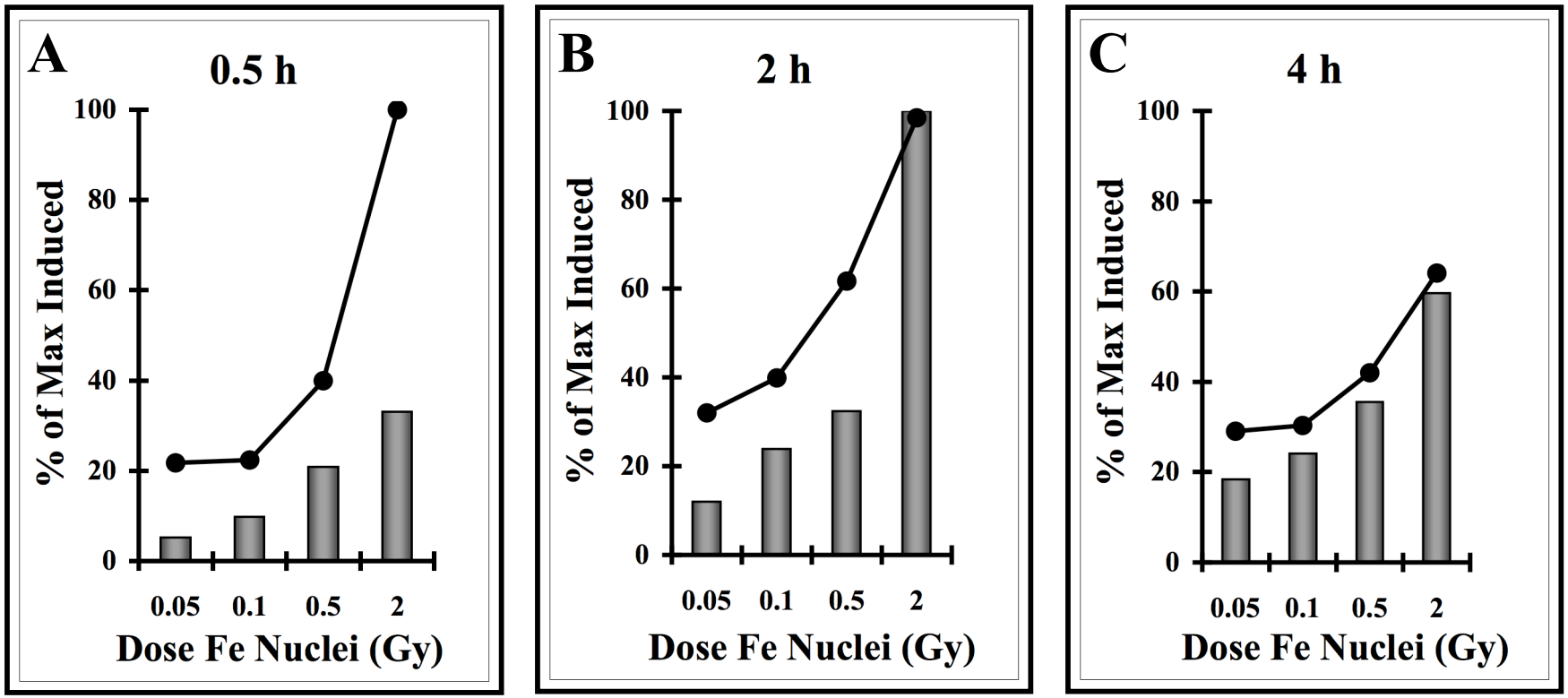
A
0.5 h
% of Max Induced
100
80
60
40
20
0
0.05
0.1
0.5
2
Dose Fe Nuclei (Gy)
B
2 h
% of Max Induced
100
80
60
40
20
0
0.05
0.1
0.5
2
Dose Fe Nuclei (Gy)
C
4 h
% of Max Induced
100
80
60
40
20
0
0.05
0.1
0.5
2
Dose Fe Nuclei (Gy)

Figure 2

Figure 3

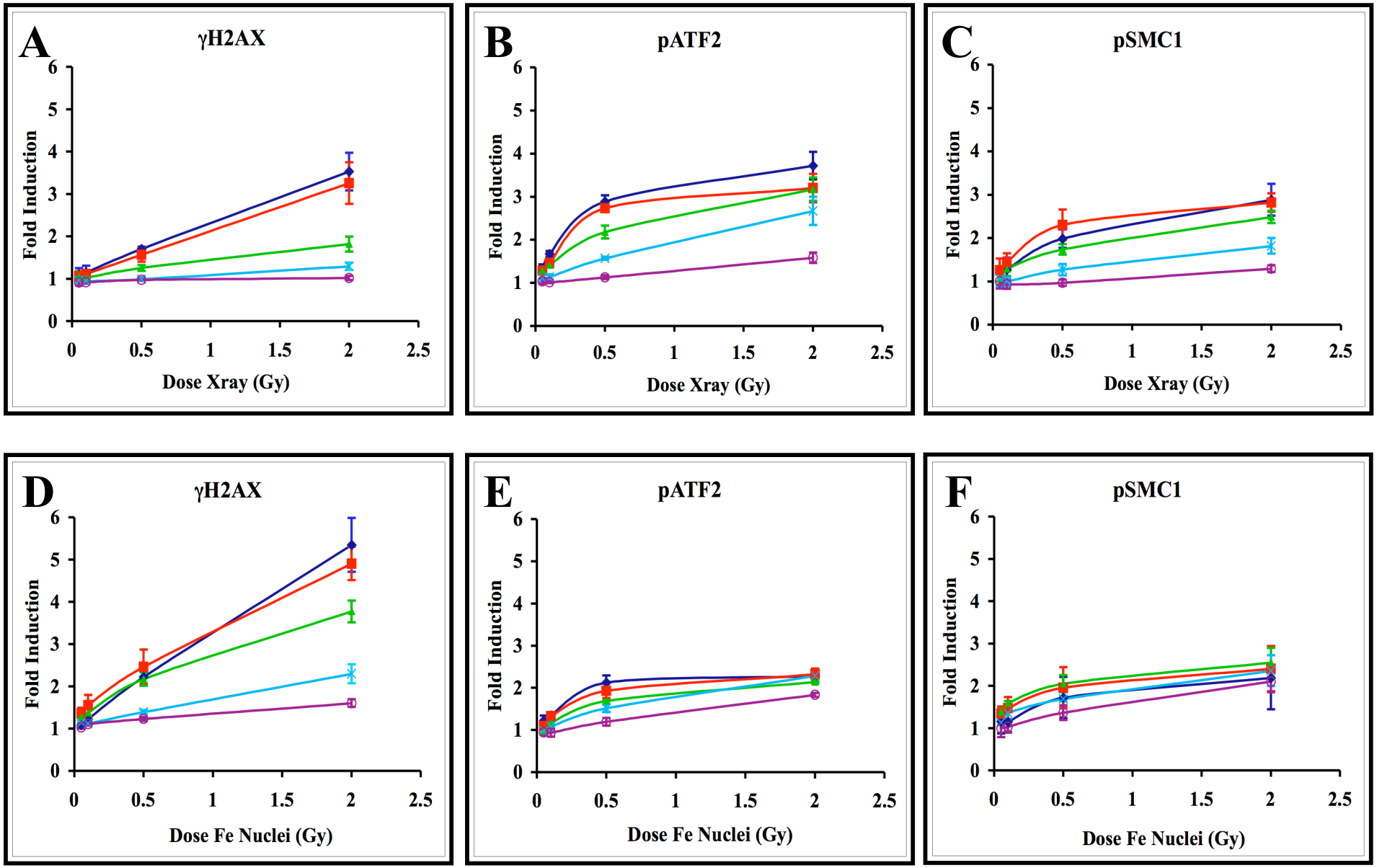
A
γH2AX
Fold Induction
Dose Xray (Gy)
B
pATF2
Fold Induction
Dose Xray (Gy)
C
pSMC1
Fold Induction
Dose Xray (Gy)
D
γH2AX
Fold Induction
Dose Fe Nuclei (Gy)
E
pATF2
Fold Induction
Dose Fe Nuclei (Gy)
F
pSMC1
Fold Induction
Dose Fe Nuclei (Gy)

Figure 4

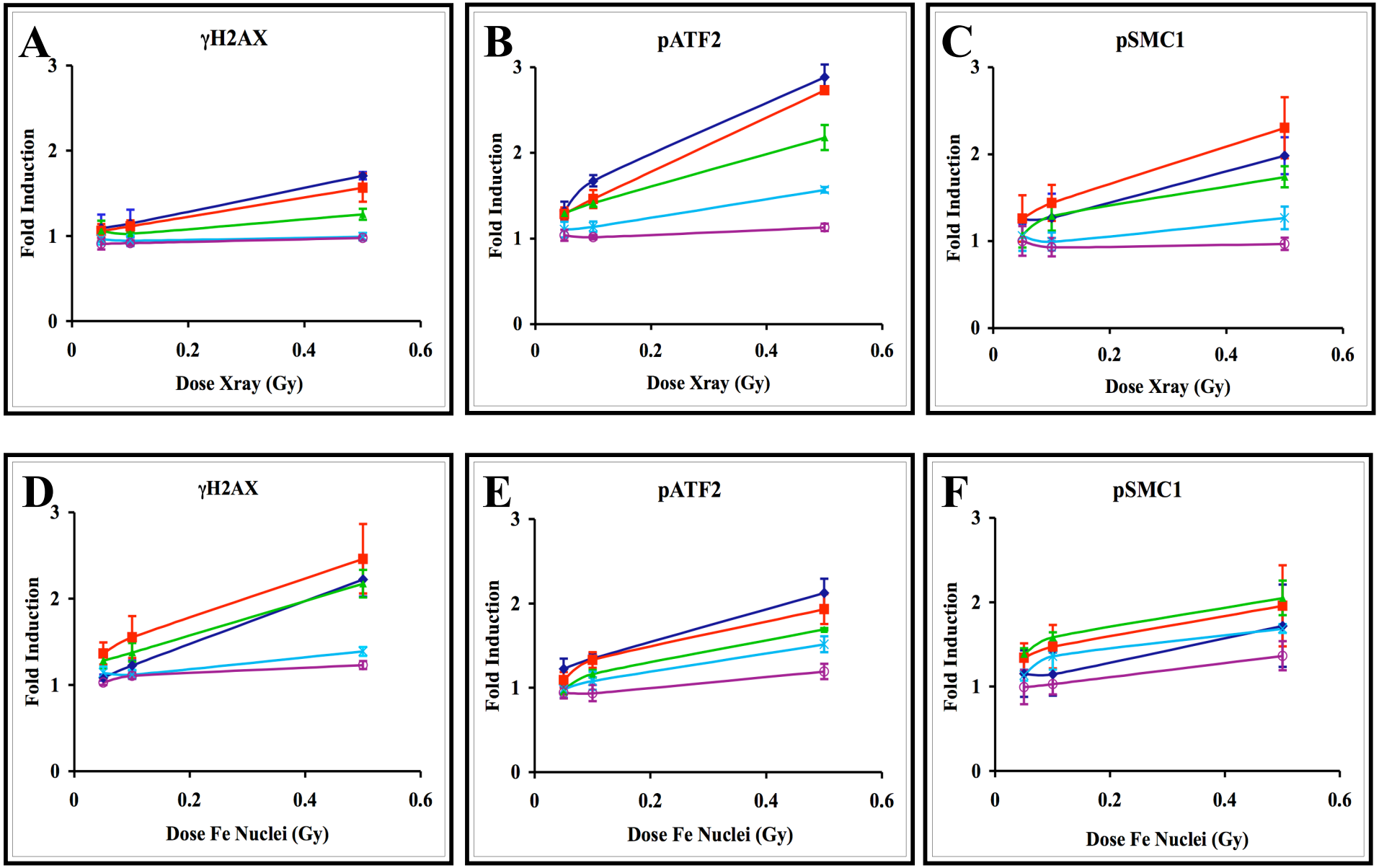
A
γH2AX
Fold Induction
Dose Xray (Gy)
B
pATF2
Fold Induction
Dose Xray (Gy)
C
pSMC1
Fold Induction
Dose Xray (Gy)
D
γH2AX
Fold Induction
Dose Fe Nuclei (Gy)
E
pATF2
Fold Induction
Dose Fe Nuclei (Gy)
F
pSMC1
Fold Induction
Dose Fe Nuclei (Gy)
0
1
2
3
0
0.2
0.4
0.6

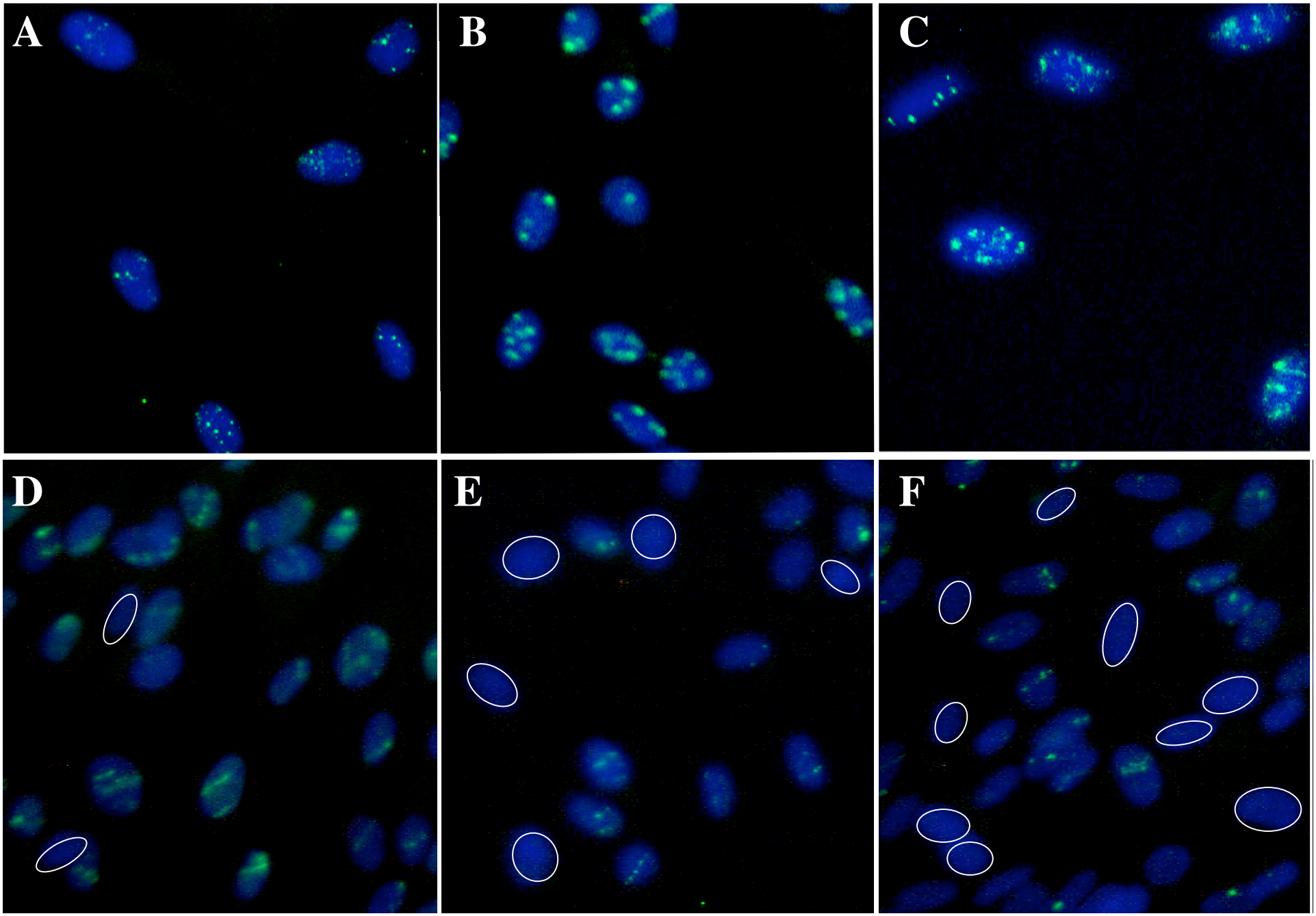

Figure 5

Figure 6

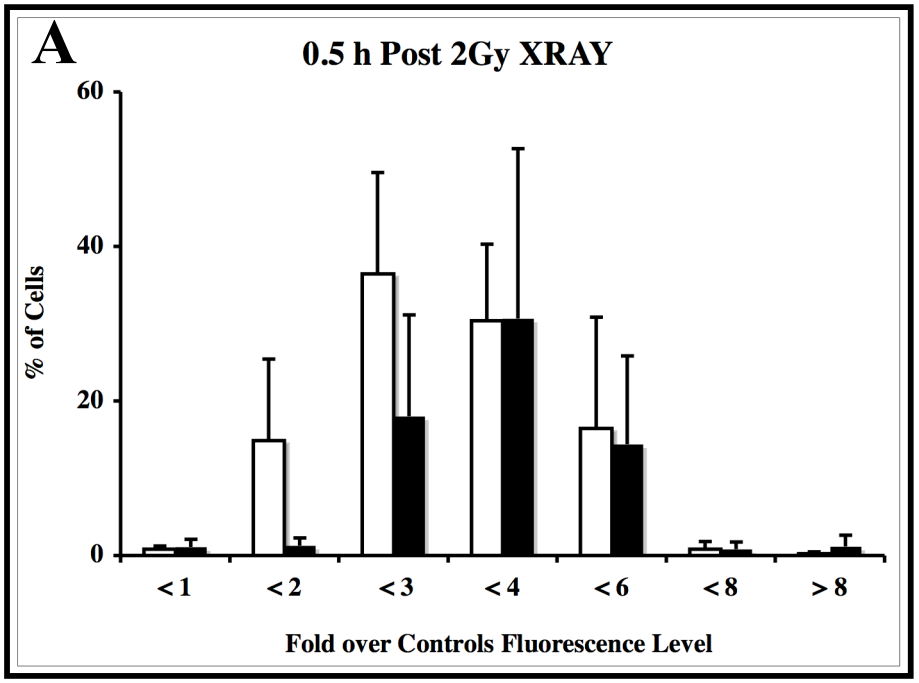
A
0.5 h Post 2Gy XRAY
% of Cells
60
40
20
0
< 1
< 2
< 3
< 4
< 6
< 8
> 8
Fold over Controls Fluorescence Level

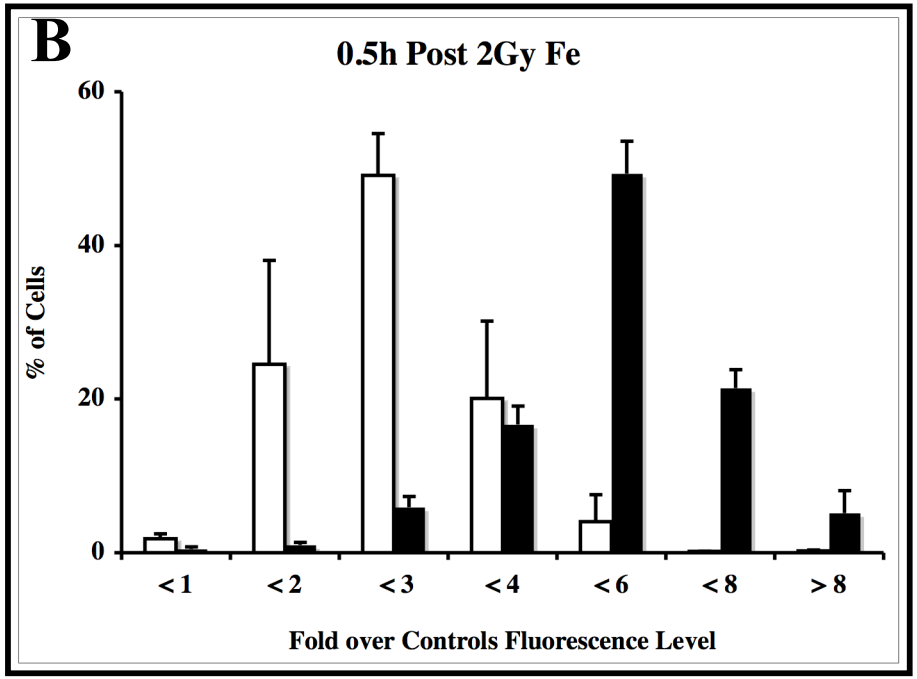
B
0.5h Post 2Gy Fe
% of Cells
60
40
20
0
< 1
< 2
< 3
< 4
< 6
< 8
> 8
Fold over Controls Fluorescence Level

Figure 7

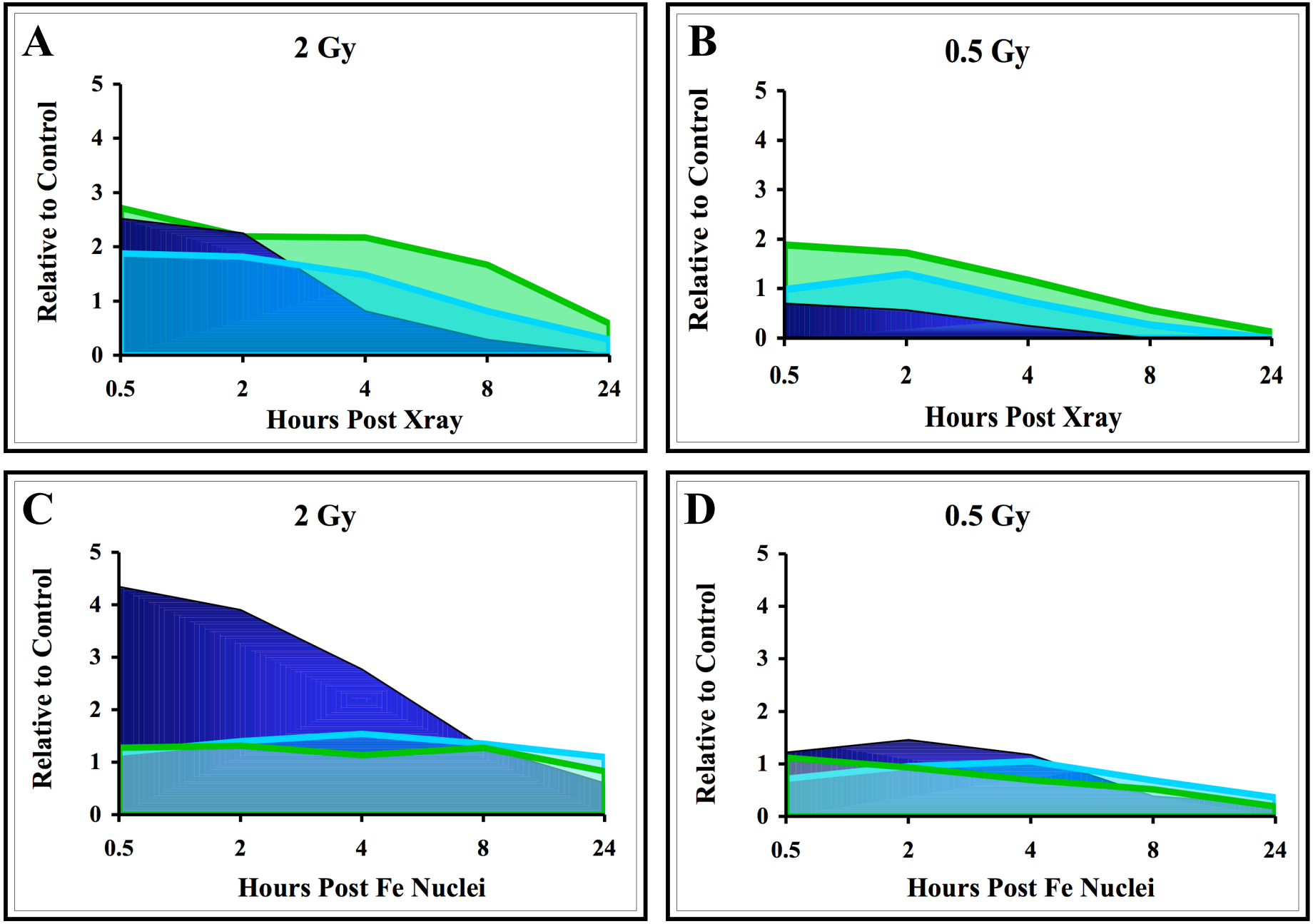
A
2 Gy
Relative to Control
0
1
2
3
4
5
0.5
2
4
8
24
Hours Post Xray
B
0.5 Gy
Relative to Control
0
1
2
3
4
5
0.5
2
4
8
24
Hours Post Xray
C
2 Gy
Relative to Control
0
1
2
3
4
5
0.5
2
4
8
24
Hours Post Fe Nuclei
D
0.5 Gy
Relative to Control
0
1
2
3
4
5
0.5
2
4
8
24
Hours Post Fe Nuclei

Figure 8

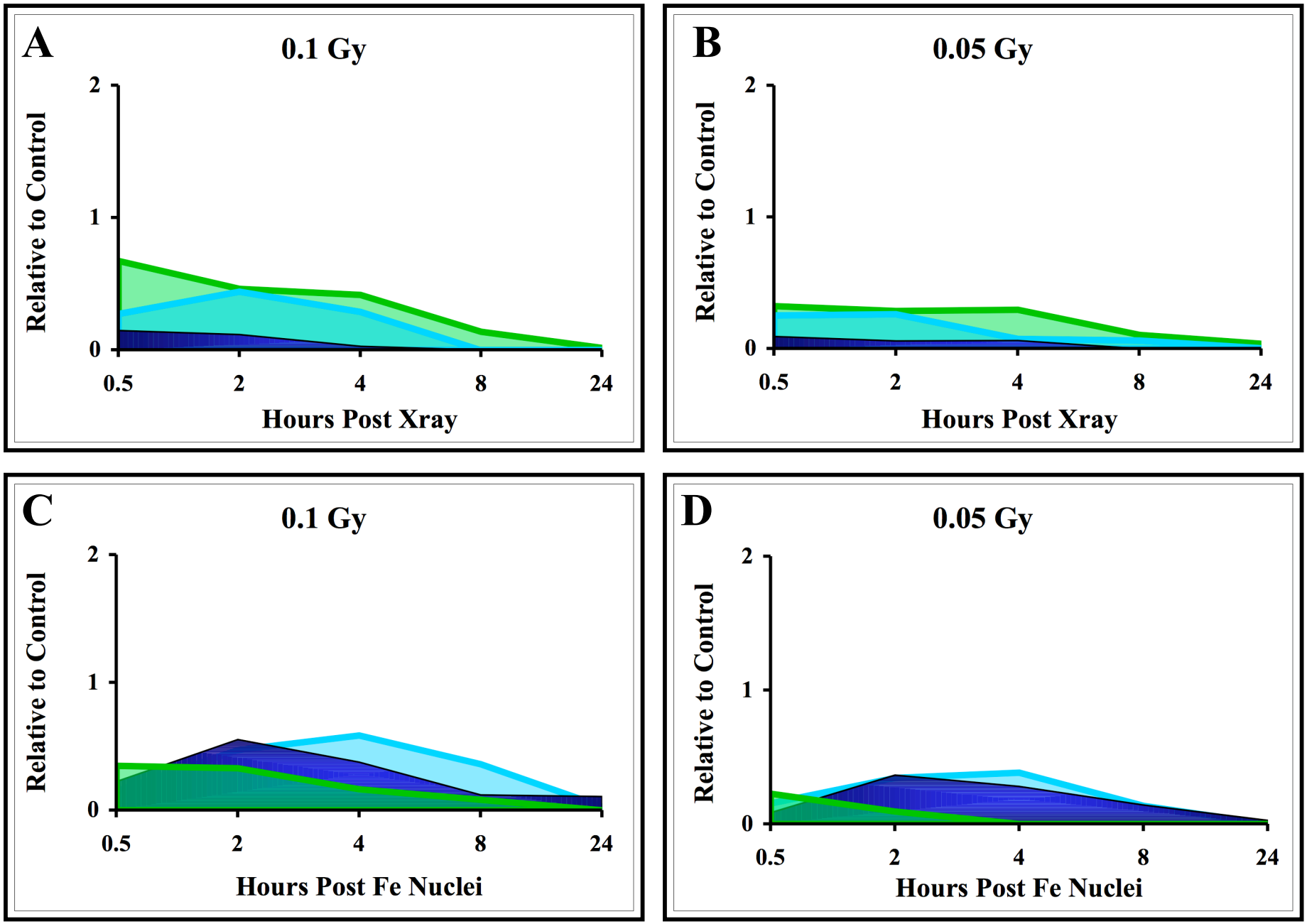
A
0.1 Gy
Relative to Control
2
1
0
0.5
2
4
8
24
Hours Post Xray
B
0.05 Gy
Relative to Control
2
1
0
0.5
2
4
8
24
Hours Post Xray
C
0.1 Gy
Relative to Control
2
1
0
0.5
2
4
8
24
Hours Post Fe Nuclei
D
0.05 Gy
Relative to Control
2
1
0
0.5
2
4
8
24
Hours Post Fe Nuclei

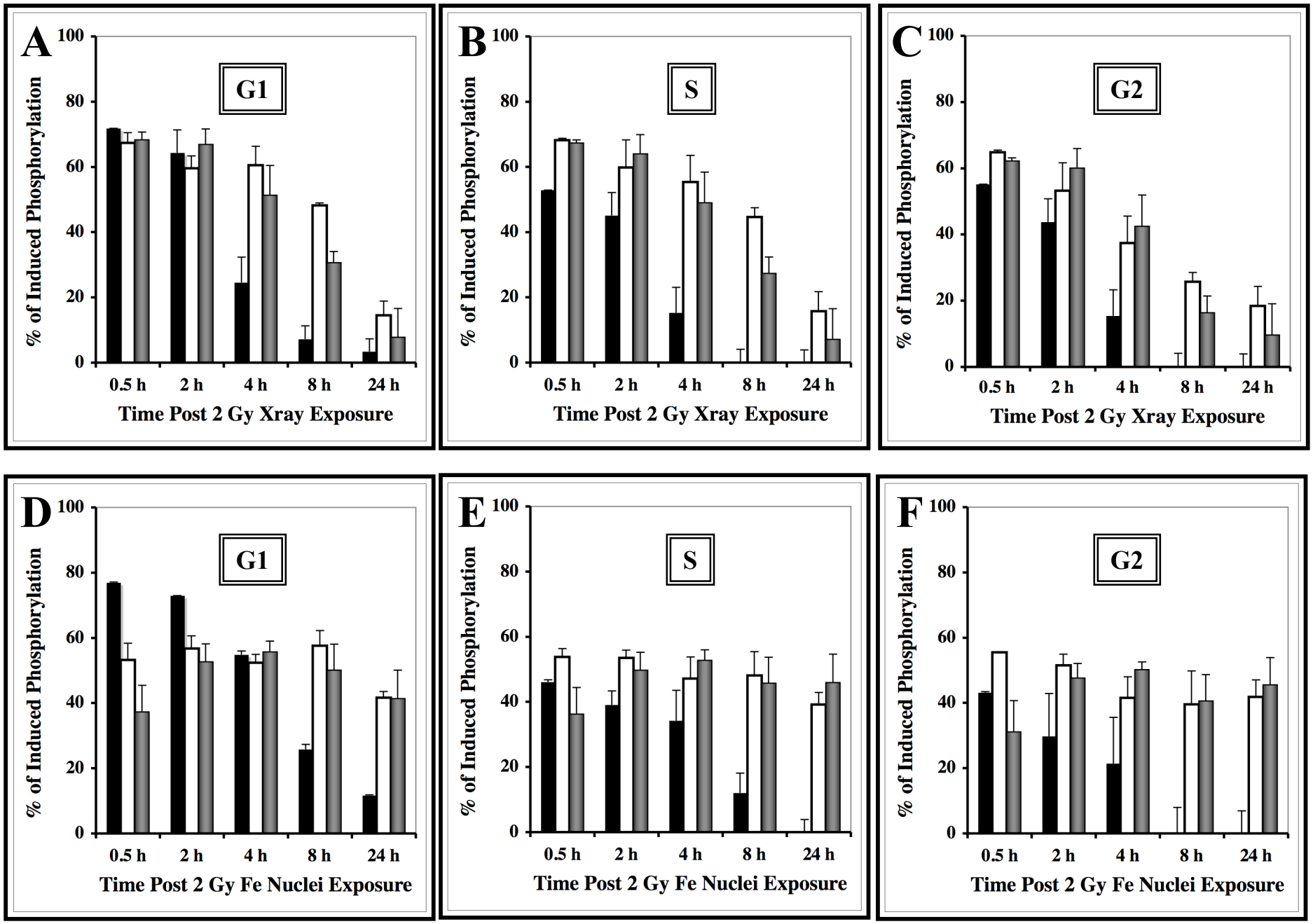
A
G1
% of Induced Phosphorylation
100
80
60
40
20
0
0.5 h
2 h
4 h
8 h
24 h
Time Post 2 Gy Xray Exposure
B
S
% of Induced Phosphorylation
Time Post 2 Gy Xray Exposure
C
G2
% of Induced Phosphorylation
Time Post 2 Gy Xray Exposure
D
G1
% of Induced Phosphorylation
Time Post 2 Gy Fe Nuclei Exposure
E
S
% of Induced Phosphorylation
Time Post 2 Gy Fe Nuclei Exposure
F
G2
% of Induced Phosphorylation
Time Post 2 Gy Fe Nuclei Exposure

Figure 9